4 Numerical performance of the long pipe roof

4.1 Numerical model

A three-dimensional model was built to simulate the real landform and ground conditions, as showed in Fig. 8. The pipe roof and surrounding rock were simulated with solid element while the primary shotcrete support was modelled with so called “liner” elements. Time-dependent strength effect of the sprayed concrete was considered by gradually increasing the strength parameters during the computation. The strength of the shotcrete is assumed to increase linearly and stabilizes after six round length of shotcrete supporting.

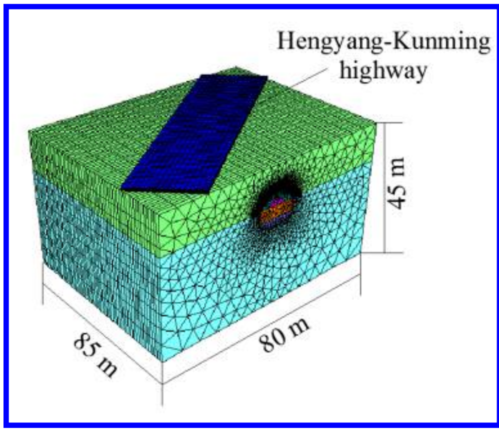

Fig. 8 3D meshed numerical model

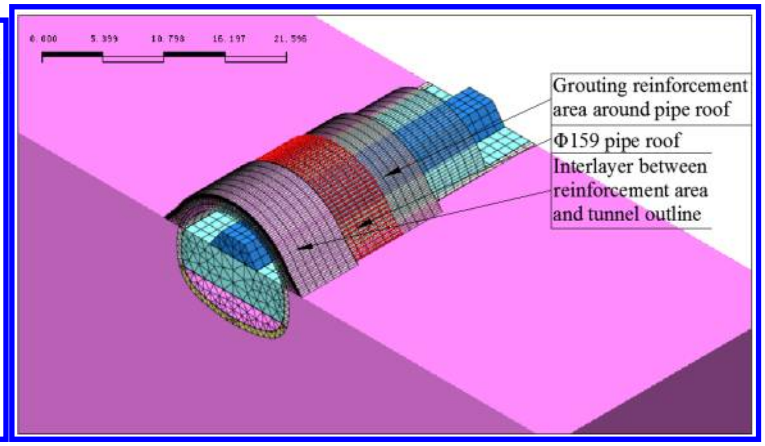

Fig.9 Detail view of meshed model

Since the diameter of the pipe roof is very small compared to the excavation section size, very fine mesh should be used for the pipe roof and the surrounding rock mass. This leads to a total number of 450 thousand solid elements. The model was first built with Midas and then imported into FLAC 3D for computation. Fig.9 shows some details of the meshed model in 3D.

The upper surface boundary of the model was free, while the four sides were horizontally constrained and the bottom surface was fixed. The ends of the pipes were rigid constrained because of they are embedded with the entrance casing arch. The highway pavement was considered as different material layers in the model. The tunnel excavation was simulated by top heading and then bench and invert excavation, with a round length of 1m, 2m and 4m, respectively. The length of core soil during the top heading was maintained to be 4-6m. The bench face was about 12-14m behind the top heading face, and the inverted face was about 12m behind the bench face. Each step of removing the soil of round length was calculated to obtain numerical equilibrium, and consequently support has been placed before the next step of excavation. Such excavation process was equivalent to the real situation and was simulated by writing FISH script in FLAC3D. Other construction effects such as blasting of the lower hard rock were not considered in this research.

The behavior of the tunnel surrounding rock was modelled by the Mohr–Coulomb failure criterion [15]. The primary support and the pipe roof were modelled as linear elastic. The physical and mechanical material parameters used in this calculation are shown in Table 1 [16]. The stiffness of the pipe roof was calculated from the steel pipe and the filled concrete, while the reinforcement in the primary support was equivalent to an increase of shotcrete stiffness.

Table 1 Material properties

Material	$\rho(kg/m^3)$	E(GPa)	υ	c(kPa)	Φ(°)	H(m)
The pavement concrete layer	2400	30	-	-	-	0.3
The pavement basic layer	2400	0.6	0.25	10	30	0.4
Soil layer	2000	0.06	0.35	20	40	0.3
Expansive soil	2000	0.03	0.35	18	20	11.2
Limestone	2600	5	0.30	600	55	33.8
First layer primary support	2400	26.4	0.2	-	-	0.55
Second layer primary support	2400	26.32	0.2	-	-	0.25
Grouting pipe roof	2500	76.5	0.2	-	-	-

Note：ρ—Density, E—Elastic Modulus, υ—Poisson, c—Cohesion, φ—Friction angle.

4.2 Numerical results

4.2.1 The stress of the pipe roof

Fig. 10 shows the longitudinal stress distribution of the selected pipe varies with the location of tunnel face. The stress of the pipe also appears to be a bimodal curve distribution. The two peak values of the stress increase and their position moves forward with the tunnel face advancing. After a certain distance of tunnel excavation, the two peak values no longer increase but move forward with the excavation of tunnel face. The pipe roof has undergone tensile stress ahead of the tunnel face. This tension length is about twice the height of top heading excavation with the maximum tensile stress at the half length. The pipe roof has undergone compression behind the tunnel face and the maximum value was at a distance equal to the top heading height behind the tunnel face. Moreover, the pipe roof near the entrance has undergone tension. The maximum tensile stress occurred close to the entrance casing arch.

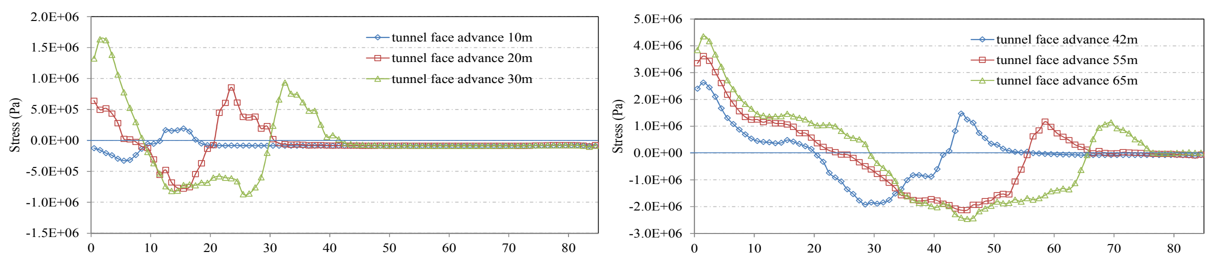

(a) The 0-30m segment of excavation (b) The 30-65m segment of excavation

Fig.10 Horizontal stress longitudinal distribution for pipe roof

Both the field measurements and the numerical analysis show that the performance of the pipe roof can be divided into three areas along the longitudinal direction. They are the tension section ahead of the tunnel face, the compression section behind the tunnel face, and the tension section near the entrance casing arch, as shown in Fig. 11.

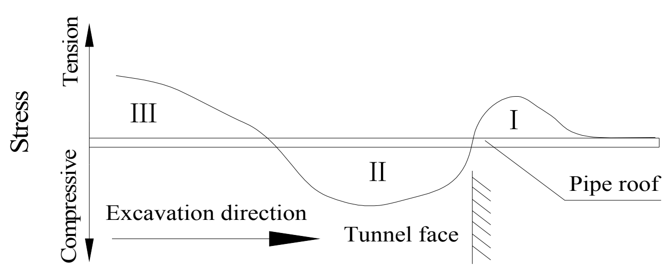

Fig.11 Zoning of longitudinal stress for pipe roof

Actually, the pipe roof in section I has undergone tension. The peak tensile stress occurred ahead of the tunnel face at a distance which is equal to the excavation height of top heading. The pipe roof in section II has undergone compression. The peak value of compressive stress occurred at a distance behind the tunnel face. This distance is about 5 m in numerical analysis while it is about 10 m in field measurements. The relative larger distance in field measurements is due to the lagging effect of the closure of the primary shotcrete in a tope heading construction method. In section III the pipe roof has undergone tension as well. The peak value of tensile stress occurred close to the entrance casing arch.

All the analysis shows that the calculated section length and the peak stress of each section vary with the distance of excavation length. The length of section Ⅱ and Ⅲ increases with the excavation of tunnel face, however, the length of section Ⅰ keeps to be a constant length. Besides, the peak stress of pipe roof in each section also increases with advancing of the tunnel face. This increase is fast at the beginning of excavation and after the excavation passed half length of the pipe roof the stress increases very slowly.

4.2.2 Comparison between field measurements and numerical results

The measured strain of the pipe was converted to stress by using the equivalent stiffness of the pipe roof, which is calculated from the elastic modulus of the steel pipe and the in-filled mortar. Fig. 12 shows the stress calculated both from field measurements and numerical analysis. The two results are found in good agreement both in values and distribution. This results show that the numerical method used in this study can serve as an effective method in modelling the performance of long and large pipe roof in tunnelling.

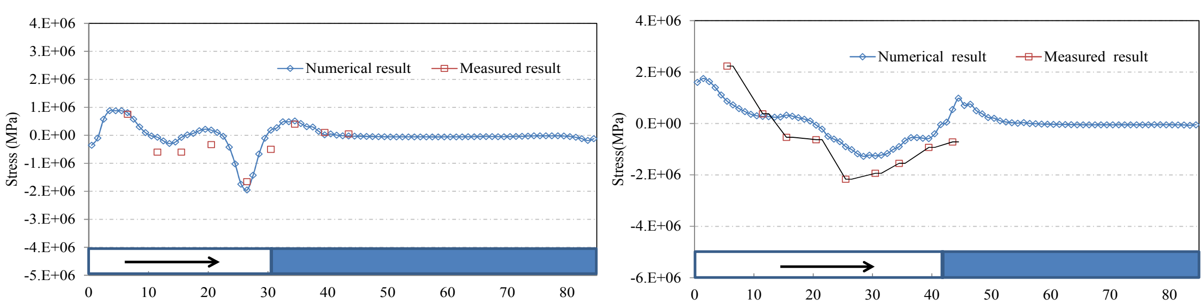

(a) Stress of the pipe with 30 m excavation (b) Stress of the pipe with 42 m excavation

Fig.12 Comparison of the pipe stress from numerical simulation and field measurements

5 CONCLUSIONS

The performance of long and large pipe roof in Shitougang tunnel was analyzed by field measurements and 3D numerical analysis. Based on the mechanical response of the typical pipe at the tunnel crown, the following conclusions were obtained:

- The development of stress along the long and large pipe roof turns out to be a bimodal curve distribution. The waveform of the distribution curve increases initially and then moves forward with the advance of the tunnel face.
- The stress distribution of the pipe roof can be divided into three sections: tension section ahead of the tunnel face, compressive section behind the tunnel face and tension section near the entrance casing arch. The peak tensile stress generally occurred near the entrance casing arch and at a distance equal to the

excavation height ahead of the tunnel face. The peak compressive stress is related to the distance from closed primary support to the tunnel face. The length of tension section which is close to the entrance casing arch tends to be constant while the other two sections vary with the tunnel face position.

- The stress of the pipe increases fast first and then it increases very slowly after the tunnel face passed the half length of the pipe roof.
- The calculated stress of pipe roof was in good agreement with the measured result. Solid elements with consideration for the contact between the surrounding rock and pipe roof can serve as an effective tool to analyze the long and large pipe roof.

Acknowledgement

The authors are grateful to the CCCC Fourth Highway Engineering Co., LTD. of China and Nanning Railway Bureau of China Railway Corporation for the contributions and support regarding the field measurements presented in this paper. The technology demonstration research project of China Ministry of Transport (CXKJSF0106-1) and the National Science and Technology Support Program of China (No. 2012BAK24B02) are also appreciated.

References

1. Barisone, G., B. Pigorini, and S. Pelizza. Umbrella Arch Method for Tunnelling in Difficult Conditions—Analysis of Italian Cases. *Proc.,4th Congress, International Association of Engineering Geology,* 1982,New Delhi, India, pp. 15-27.
2. Ibrahim, O. Control of Surface Settlements with Umbrella Arch Method in Second Stage Excavations of Istanbul Metro. *Tunnelling and Underground Space Technology*, Vol. 23, 2008, pp.674-681.
3. C.O. Aksoy, and T. Onargan. The Role of Umbrella Arch and Face bolt as Deformation Preventing Support System in Preventing Building Damages. *Tunneling and Underground Space Technology*, Vol. 25, 2010, pp.553-559.
4. Volkmann, G., and W. Schubert. Optimization of Excavation and Support in Pipe Roof Supported Tunnel Sections. *Tunneling and Underground Space Technology*, Vol. 21, 2006.
5. The Professional Standards Compilation Group of People's Republic of China (JTG D70－2004). *Code for Design of Road Tunnel*. China Communications Press, Beijing, 2004.
6. Yoo, C. Finite Element Analysis of Tunnel Face Reinforced by Longitudinal Pipes. *Computers and Geotechnics*, Vol.29, 2002, pp.73-94.
7. Yoo, C., and Shin, H.K. Deformation Behavior of Tunnel Face Reinforced with Longitudinal Pipes Laboratory and Numerical Investigation. *Tunneling and Underground Space Technology*, Vol.18, 2003, pp.303-319.
8. Tan, W. L., and P. G. Ranjith. Numerical Analysis of Pipe Roof Reinforcement in Soft Ground Tunneling. Proc., 16th International Conference on Engineering Mechanics (CD-ROM), 2003, ASCE, Seattle, Wash.
9. Hefny, A. M., W. L. Tan, P. Ranjith, J. Sharma, and J. Zhao. Numerical Analysis for Umbrella Arch Method in Shallow Large Scale Excavation in Weak Rock. Tunneling and Underground Space Technology, Vol. 19, 2004.
10. Galli G, Grimaldi A, and Leonardi A. Three-Dimensional Modelling of Tunnel Excavation and Lining. *Computers and Geotechnics,* Vol. 31, No.3, 2004, pp.171-183.
11. Bae, G. J., J. S. Shin, C. Sicilia, Y. G. Choi, and J. J. Lim. Homogenization Framework for Three-Dimensional Elastoplastic Finite Element Analysis of a Grouted Pipe-Roofing Reinforcement Method for Tunneling. *International Journal for Numerical and Analytical Methods in Geomechanics,* Vol. 29, No. 1, 2005, pp. 1-24.
12. Shin, J.H., Y.K. Choi, O.Y. Kwon et al. Model Testing for Pipe-Reinforced Tunnel Heading in a Granular Soil. *Tunneling and Underground Space Technology,* Vol. 23, 2008, 241-250.
13. Yang, J.S., D.M. Gou and Y.X. Zhang. Field Measurements and Numerical Analyses of Double-layer Pipe Roof Reinforcement in a Shallow Multiarch Tunnel, *Journal of Transportation Research Record (No. 2050/Structures)*: 2008, pp.145-153.
14. ZHENG, J., R. ZHANG and Q. YANG. Mechanical Mechanism of Pipe Roofs with Variable Coefficient of Subgrade Reaction in Shallow Tunnels. *Chinese Journal of Geotechnical Engineering*, Vol. 31, No. 8, 2009.
15. FLAC User's Manual, Version 5.0. Itasca Consulting Group, Inc., Minneapolis, Minn., 2005.
16. China Railway Eryuan Engineering Group CO.LTD. Survey and Design Report of Shitougang Tunnel of Bid Section Ⅱ of Extension Project of Hunan and Guangxi Railway. Chengdu, 2009.

Analysis of the Impacts of a Tunnel on a Normal Fault Rupture through Uniform Soil Cover

Mehdi Sarayloo[1] and Reza Mahinroosta[2]

[1]Dept. of Civil Engineering, Zanjan Branch, Islamic Azad Univ., Zanjan, Iran. E-mail: m_sarayloo@yahoo.com
[2]Lecturer, Engineering, Engineering Faculty, Charles Sturt Univ., Panorama Ave BATHURST, NSW 2795, Australia. E-mail: rmahinroosta@csu.edu.au

Abstract: Damages due to a fault activity can be divided into dynamic rupture and quasi-static rupture. In some special projects like roads, channels, and pipelines, engineers have to design and construct them on the faults inescapably. In addition to seismic design, the effects of fault rupture crossing the structures must be considered in the design process. In this paper, four different computer models of a granular alluvium with and without tunnel were made by a three-dimensional finite-difference software. A normal fault offset with three different cross angles was applied to the bottom of the models at the next step. Then, the shear bands propagation and ground deformations were calculated. The results show that the effects of tunnel existence on the ground deformations and shear band propagation depend on the cross angle.

INTRODUCTION

In a seismic event, the rupture of an earthquake fault generates two types of ground displacement: permanent quasi-static offsets on the fault itself, and transient dynamic oscillations away from the fault (Anastasopoulos et al. 2007). The permanent offset on a fault affects the ground surface only in some cases, when the fault rupture extends all, or nearly all the way to the surface. Naturally, over the last four decades, much less effort had been devoted to understand how a fault rupture affects the overlying soil, structures and facilities until the three notorious earthquakes of 1999 in Turkey and Taiwan having offered numerous examples of detrimental effects of large surface fault ruptures (Loukidis et al. 2009, Anastasopoulos and Gazetas 2010).

The existence of active faults in the path of tunnels implies a seismic hazard, which can affect underground and on-ground structures in addition to the tunnel. To this extent, seismic codes correctly require that the construction not be built within the ‘‘immediate vicinity’’ of active faults, at least not without a specialized analysis and design. However, the quantitative indications for the width of these set-back zones are few and rather uncertain. Given that various conditions such as a structure existence can deflect the path of shear bands in the overlying soil, the width of the set-back zone can’t be defined precisely. So for these cases, the following questions are raised:

1) Will the fault rupture reach the ground surface and at which location?
2) How will the ground surface be distorted when a tunnel exists?

This paper studies the special case of a normal fault. The numerical analyses presented herein are quasi-static, i.e. they do not account for the potential effects of seismic wave propagation and ground response.

METHODOLOGY

The numerical analyses presented herein were performed using the finite-difference code FLAC 3D, which employs the dynamic relaxation technique. The merits of the dynamic relaxation technique, in connection with the numerical analysis of fault trace propagation problems, have also been demonstrated in the previous studies (Roth et al. 1982). In this study, firstly a simple alluvium model was made, and fault displacement was applied. Then, the same fault offset was applied to the same alluvium with a tunnel for different cross angles. Finally, shear bands causing ground deformations and distortions were calculated and compared. As well as the mentioned models, two different models based on Lin et al. (2007) sandbox tests were conducted to verify the modeling method.

Verification

In this part, the two numerical models with similar characteristics with that of Lin et al. (2007) sandbox tests, were conducted in FLAC 3D and then the results were compared with theirs. They also made numerical models with FE code software (ABAQUS) the same as the physical tests. Faulting in a free-field alluvium was depicted in Figure 1 and the one in alluvium with a tunnel was depicted in Figure 2.

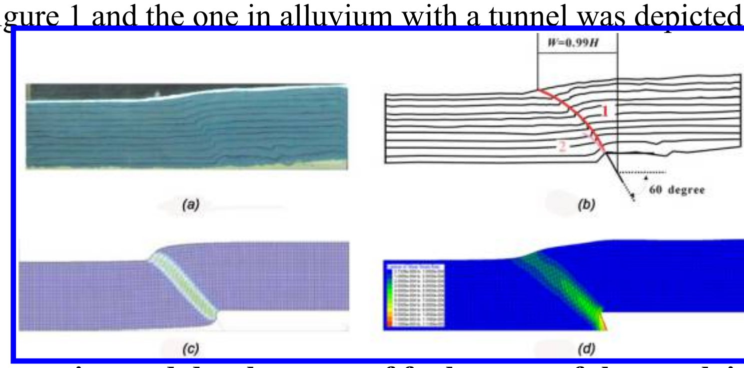

FIG. 1. Deformation and development of fault zones of the overlying overburden soil. (a) Sandbox test; (b) Sandbox test in detail; (c) FE model; (d) FD model.

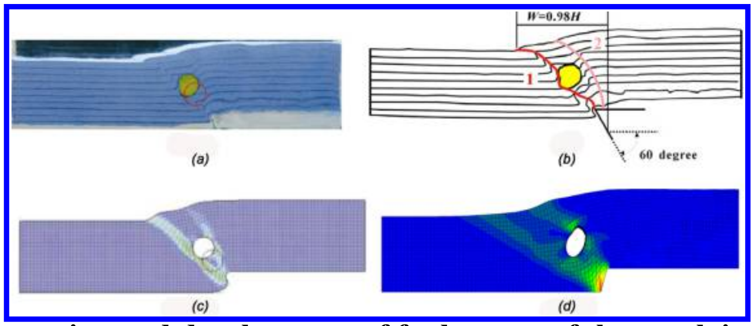

FIG. 2. Deformation and development of fault zones of the overlying overburden soil with underground tunnel. (a) Sandbox test; (b) Sandbox test in detail; (c) FE model; (d) FD model.

The similarity in shear bands development and the shape of settlements between the illustrations verifies the modeling method of this paper. Even it can be seen in Figure 1 that the results of FD model are more accurate than those of FE model in this problem.

Mesh and Boundary Conditions

The alluvium depth chosen in this study was 20 m while the length in both X and Y axis was four times bigger than the depth (i.e. 80 m) to reduce the boundary condition effects on results. In order to mesh the alluvium, a grid with a different element density was used. The tunnel excavated in the second step has a 5 m diameter and 10 m depth. The tunnel is lined with concrete segments, which were modeled by the liner elements and were connected to the grid through an interface.

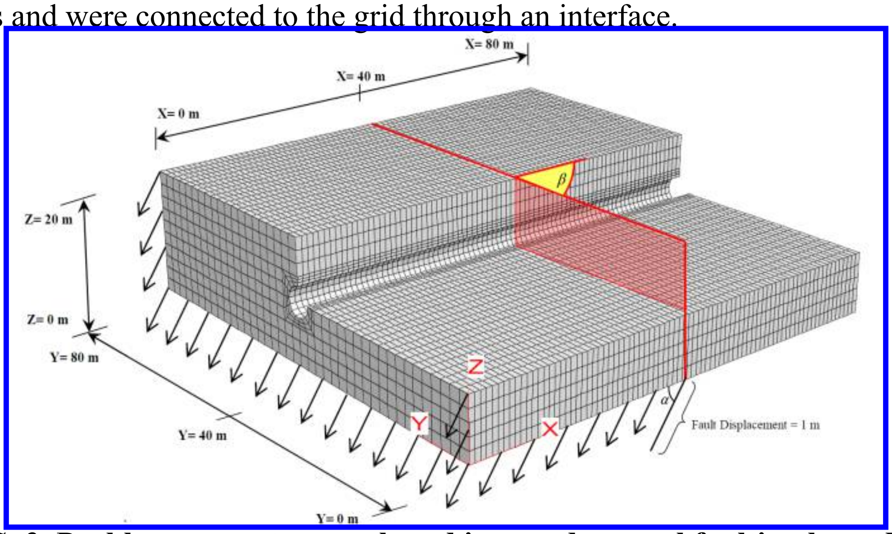

FIG. 3 Problem geometry, mesh and imposed normal faulting boundary conditions; β=Cross angle α=Fault dip angle (Sarayloo 2011).

The boundary walls of the model are fixed in their normal direction and are free in other directions. The bottom boundary is split in two parts, one that remains firm and the other follows the hanging wall movement of the fault (Figure 3). The displacement specified to the bottom boundary and boundary walls of the moving block are parallel to the fault plane in the bedrock, i.e. their direction is inclined at a dip angle α=30° relative to the horizon. The modeling is conducted for the three cross angles of β=0°, 45°, 90° and the one-meter downward fault displacement along the slide surface.

Materials Behavior

Several experimental and numerical studies have shown that post-peak soil behavior is a decisive factor in fault rupture propagation and its possible emergence on the ground surface (Anastasopoulos et al. 2007).The constitutive model assigned to the soil is the elastoplastic Mohr-Coulomb with isotropic strain-softening model. Furthermore, the studied alluvium is made of sand with low cohesion. The features of the alluvium material are mentioned in Table 1. The constitutive model assigned to the concrete lining is also elastic and is shown in Table 2.

Table 1. Parameters of the MC model used for the soil.

Model Constant	ρ (t/m^3)	E (kPa)	ν	c_p (kPa)	c_{res} (kPa)	Φ_{Ini}	Φ_p	Φ_{res}	Ψ_{Ini}	Ψ_p	Ψ_{res}
Value	2	4×10^4	0.3	1	0.75	20°	45°	30°	-11°	5°	0°

Table 2. Parameters of the MC model used for the concrete lining.

Parameter	E (kPa)	ν	f_c (kPa)	f_{ct} (kPa)	Thickness (m)
Value	2×10^7	0.2	2.5×10^4	2.5×10^3	0.5

NUMERICAL ANALYSIS

Various studies (Roth et al. 1982, Bray et al. 1994, Lin et al. 2006, Anastasopoulos et al. 2007, Loukidis et al. 2009) have been done about the fault rupture propagation in the overlying soil and the effect of different parameters such as friction angle, dilation angle, cohesion, soil type, fault type, etc. In most of these studies (Lin et al. 2006, Anastasopoulos et al. 2007, Loukidis et al. 2009), centrifuge tests or sand box tests have been used to verify the modeling. The results show the accuracy of numerical modeling and indicate the ability of these methods in predicting the fault effects on soil and structures. Some studies have been done (Shahidi and Vafaeian 2006, Lin et al. 2007, Anastasopoulos et al. 2008, Anastasopoulos and Gazetas 2010, Mahinroosta and Mirmoayed 2011) about the impact of fault rupture on structures located in the alluvium cover of the fault. Valuable results have been conducted, but because of 2D modeling, the probable cases of faulting have been limited and in fact, some cases have not been investigated.

Free-Field Alluvium

Fault rupture can cause the development of the primary shear band and a secondary shear band which are approximately symmetrical (Figure 4a).

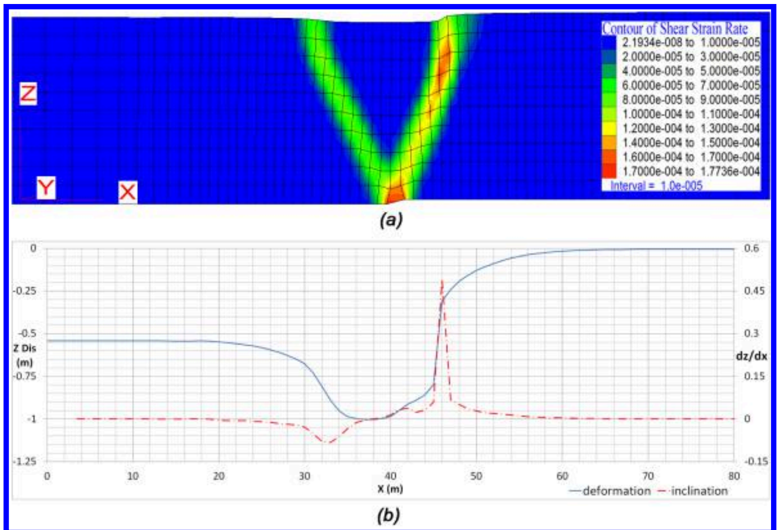

FIG. 4 One-meter fault offset with a 30° dip angle. (a) Shear bands propagation through overlying soil; (b) Ground surface settlement and inclination plot.

Usually in normal faults with small dip angles, depending on the soil type, a wedge-shaped depression can be seen on the ground surface, made by the development of the secondary shear band. This wedge failure can be seen in Figure 4a. According to the fault dip angle, the fault trace is predicted to appear at X=74.6 m but based on Figure 4b, the fault trace appears at X=46 m, indicating an average angle of faulting of 73°. Actually, the rupture propagation path is deflected in soil and becomes closer to the perpendicular. This deviation is due to the rupture path which passes through the soil. According to Figure 4b the maximum inclination is 0.49, which occurs at X=46 m and the maximum settlement is 1 m, which is 2 times larger than the fault's vertical displacement (0.5 meter), at X=37 m.

Alluvium with tunnel

Previous studies (Shahidi and Vafaeian 2005, Lin et al. 2007, Anastasopoulos et al. 2008, Anastasopoulos and Gazetas 2010) show that having a tunnel in the path of a fault rupture changes the path and the fault trace. In the second part of this study, the alluvium of the previous part is modeled with an excavated tunnel in it for different cross angles of β=0°, 45°, 90° (0° for faulting along the tunnel and 90° for faulting perpendicular to the tunnel). For more accurate modeling, the tunnel has been modeled using step by step excavation and lining method.

Faulting with a cross angle of β=0°

As shown in Figure 5a, the development of shear bands has been changed because of the tunnel. After the primary shear band reaches the tunnel perpendicularly, it is distributed on half of its circumference and then from the upper left corner it reaches the ground surface with an angle near to perpendicular. The primary shear band affects the bottom and the left walls of the tunnel. The secondary shear band is also developed which reached the surface with a similar angle in the previous section. Figure 5a shows that the wedge failure is formed above the tunnel on the left which has a smaller base width than the wedge failure formed in the free-field alluvium.

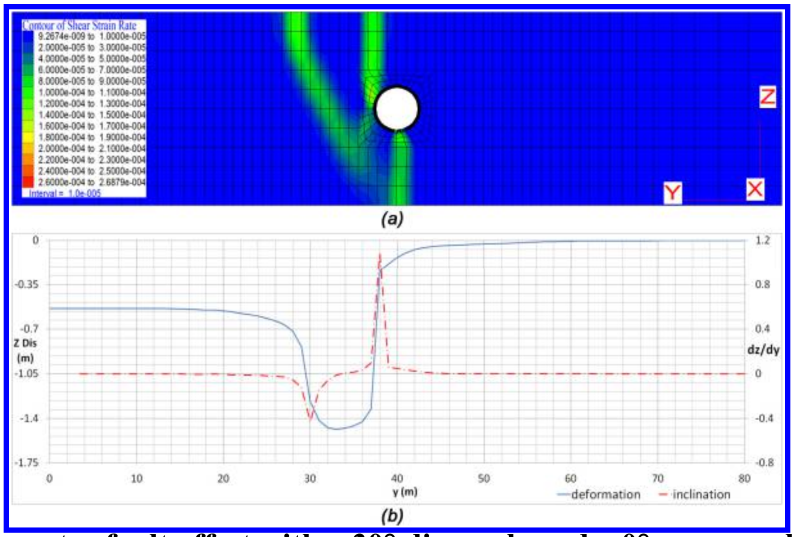

FIG. 5 One meter fault offset with a 30° dip angle and a 0° cross angle above the tunnel. (a) Shear bands propagation through overlying soil; (b) Ground surface settlement and inclination plot.

According to the tunnel existence and the deviation of the primary shear bands development, the fault trace appears at Y=38 m on the ground (Figure 5b). The maximum settlement is 1.48 m, which is 2.96 times larger than the fault's vertical displacement and appears at Y=33 m (Figure 5b). Since the wedge failure has a smaller width in this state, a smaller zone is affected by the fault rupture and so the ground surface inclination is larger than the free-field alluvium case. As shown in Figure 5b, the maximum ground surface inclination magnitude is 1.08, which is 2.2 times greater than that of the free-field alluvium state and occurs at Y=38 m.

Faulting with a cross angle of β=45°

In this case, because of the specific cross angle, in order to reduce the boundary condition's effects on the results, 20 meters were added to both sides of the model in the X direction. For this condition, the development of shear bands after reaching the tunnel, are distributed along the tunnel so that the fault rupture does not reach the ground surface (Figure 6a). The cause of this phenomenon is the angle between the tunnel and the fault trace (named cross angle), causing the tunnel to behave like a continuous beam against the fault induced movement. Therefore, the stresses caused by faulting are distributed in a longer area, and this situation does not allow the shear bands to reach the ground surface. The primary shear band affects the walls and the bottom of the tunnel when it reaches the tunnel, and like the previous state, it causes an increase in the stresses, especially tensile stresses in the concrete lining. As shown in Figure 6a, the wedge failure is only formed under the tunnel.

The maximum ground surface settlement recorded above the tunnel is 0.21 m, which is 2.38 times smaller than the fault's vertical displacement and occurs at X=43 m. The maximum inclination in this path is 0.0078, which occurs at X=45 m. (Figure 6b)